NONLINEAR SHORT-TERM UPPER OCEAN CIRCULATION VARIABILITY IN THE TROPICAL WESTERN PACIFIC

By Bo Qiu, Shuiming Chen, Brian S. Powell, Patrick L. Colin, Daniel L. Rudnick, and Martha C. Schönau

ABSTRACT. Due to the presence of a well-defined permanent thermocline, low-frequency upper ocean circulation variability in the tropical western Pacific Ocean is effectively captured by the region's linear baroclinic Rossby wave dynamics. A careful examination of variations in the circulation surrounding Palau using in situ temperature measurements, satellite altimetry data, and ECCO2 (Estimating the Circulation and Climate of the Ocean, Phase II) ocean state estimates reveals that linear dynamics fails to describe the observed large-amplitude upper ocean variations on monthly timescales. These short-timescale variations are particularly active during the transition from El Niño to La Niña conditions. As an El Niño event terminates and the tropical trade winds rebound, downwelling baroclinic Rossby waves are generated across the off-equatorial Pacific basin. When these wind-forced Rossby waves propagate into the western North Pacific basin, they deform the pre-existing, horizontally sheared, North Equatorial Countercurrent (NECC) and subject it to barotropic instability. By breaking down into large-amplitude eddies, the unstable NECC generates rapidly evolving upper ocean changes with sea level, temperature, and meridional velocity fluctuations exceeding 0.5 m, 10°C, and 0.5 m s^{-1}, respectively, over a period of one to two months around Palau. This variability in short-term, large-amplitude upper ocean circulation results in significant regional water mass and ecosystem changes.

IN PLAIN WORDS. During the transition period from El Niño to La Niña conditions, reestablished trade winds generate large-amplitude, westward-propagating, perturbations in the velocity of upper ocean currents. When these wind-generated perturbations reach the Philippine Sea in the western Pacific, they lead to a breakdown of the North Equatorial Countercurrent and result in regional sea level, near-surface water temperature, and velocity changes exceeding 0.5 m, 10°C, and 0.5 m s^{-1}, respectively, within one to two months. These short-term upper ocean fluctuations can significantly impact regional water mass properties and cause ecosystem changes.

INTRODUCTION

Combined wind and buoyancy forcing at the sea surface across the Pacific basin creates a well-developed permanent thermocline in the tropical Pacific that separates the upper ocean, typically to a depth of 300 m, from the underlying abyssal ocean. In the low latitudes where the Coriolis parameter f is small, the tropical Pacific Ocean also has a relatively large baroclinic deformation radius in the 100–200 km range (Chelton et al., 1998). These two factors result in large spatial and small temporal scale upper ocean circulation variability in the tropical Pacific Ocean. By taking advantage of these factors, in the past, many theoretical and numerical studies have adopted the simple linear 1½-layer reduced-gravity (RG) model to explore this variability. For example, these studies have focused on the variations of regional sea level (e.g., Timmermann et al., 2010; Qiu and Chen, 2012; Greatbatch et al., 2018); prominent regional currents such as the North Equatorial Current (NEC), the North Equatorial Countercurrents (NECC), and the South Equatorial Current (SEC) (e.g., Kessler, 1990; Qiu and Joyce, 1992; Hsin and Qiu, 2012; Kessler and Cravatte, 2013); and flow fluctuations along the western boundary, such as the NEC bifurcation (e.g., Qiu and Chen, 2010; Zhuang et al., 2013; Cabrera et al., 2015).

While linear vorticity dynamics provides an adequate framework for quantifying the low-frequency circulation variability with periods > O(100 days) and horizontal scales > O(hundreds of kilometers), shorter timescale variability in the tropical western Pacific Ocean can also bring about drastic changes in regional sea level and upper ocean thermal structures. Figure 1 provides a good example of shorter timescale variability, showing a time series of upper ocean water temperatures observed on the outer slopes of Palau's eastern and western barrier reefs (Figure 1a; Colin, 2018). In many instances, such as in March 2010 and March 2016, the three-day mean water temperature increase at 90 m depth can exceed 10°C within a two-month period. Such large-amplitude temperature "swings" can significantly impact regional coral reef ecology and bleaching (Bruno et al., 2001; Colin, 2009, 2018; Schramek et al., 2018). Not coincidentally, these large-amplitude upper ocean water temperature changes are reflected in sharp regional sea level fluctuations at Palau with warmer (colder) temperatures corresponding to higher (lower) sea level (see Figure 1c). Quantitatively, the water temperature changes in the upper 90 m layer can contribute about 30% of regional sea level fluctuations.

In addition to the water temperature and sea level changes shown in Figure 1b,c, the upper ocean circulation around Palau also exhibited corresponding large-amplitude fluctuations. Figure 1d shows daily meridional surface velocity fluctuations based on AVISO west off Palau at 7.25°N, 134.25°E. The velocity fluctuations have a standard deviation of 13.9 cm s^{-1}. Large northward flows, with amplitudes exceeding three standard deviations, were detected in 2001, 2010, and 2016. In Figure 1b, these anomalously intense northward flows originating from the NECC are responsible for the sharp upper ocean warmings evident in early 2010 and 2016.

It is worth noting that the multi-faceted, large-amplitude upper ocean changes shown in Figure 1b–d are detected during the transition periods from the El Niño to La Niña conditions in the tropical Pacific Ocean. As such, they represent the interannual upper ocean variability that can

FACING PAGE. Shallow reef off Palau. (top) High coral cover shallow reef at high tide during El Niño-Southern Oscillation neutral sea level conditions on July 25, 2013. (bottom) The same reef on January 7, 2016, after a period of El Niño low mean sea level conditions, which exposed the uppermost branches of coral to air for extended periods and caused their death. *Photo credit: Patrick L. Colin, CRRF*

be partially captured by the large-scale, wind-forced circulation changes based on the linear vorticity dynamics. As this study demonstrates, the linear vorticity dynamics-based evaluation of the upper ocean circulation fluctuations tends to significantly underestimate the observed short-term (i.e., monthly timescale) fluctuations. The objectives of this study are twofold. The first objective is to provide large-scale upper ocean circulation variability context for intensive near-field observations conducted around Palau during 2016–2017 as part of the Office of Naval Research (ONR) Departmental Research Initiative (DRI) project Flow Encountering Abrupt Topography (FLEAT). Regarding this objective, our study complements the articles of Schönau et al. (2019), Andres et al. (2019), and Zedler et al. (2019) in this issue. The second objective of this study is to quantify the relative importance of basin-scale wind-forced variability in circulation versus that induced by nonlinear dynamical processes that originate from the interaction between the wind-forced baroclinic Rossby waves and the background NECC in the tropical western Pacific Ocean. A better understanding of nonlinear oceanic processes is essential for predicting the large-amplitude, short-term variability that is ubiquitous in the tropical western Pacific Ocean.

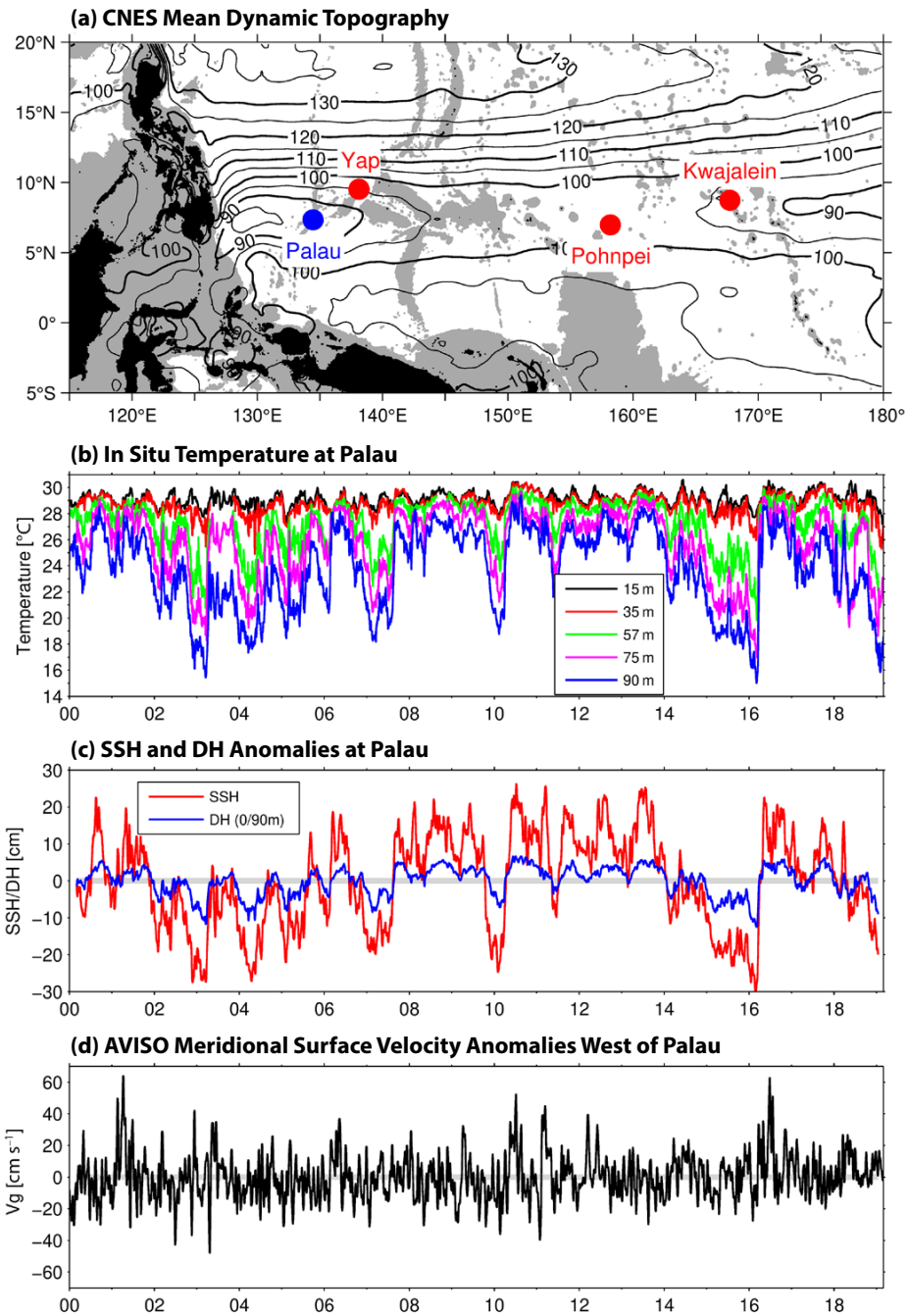

FIGURE 1. (a) Mean dynamic topography (solid contours in cm) in the tropical western Pacific Ocean compiled by the French space agency CNES (Rio et al., 2014). Gray shades indicate areas where the ocean depth is shallower than 3,000 m. (b) In situ three-day mean water temperature data observed at Short Drop Off (7°16'N, 134°31'E) and Ulong Rock (7°17'N, 134°52'E), Palau. (c) Time series of sea level anomalies from AVISO (red line) and of the dynamic height (DH) calculated from the water temperature data of (b) with a reference level at 90 m. (d) Time series of meridional surface velocity anomalies from AVISO west of Palau at 7°15'N, 134°15'E.

REDUCED-GRAVITY MODEL AND ECCO2 OCEAN STATE ESTIMATE

To quantify the relative importance of the linear vs. the nonlinear processes, we adopt two approaches. For the linear process, we use the 1½-layer RG model that governs the linear, wind-driven upper layer circulation variability. The governing equations of the model (Gill, 1982) are

$$\frac{\partial \mathbf{u}}{\partial t} + f\,\mathbf{k} \times \mathbf{u} = -g'\nabla h + A_h \nabla^2 \mathbf{u} + \frac{\boldsymbol{\tau}}{H\rho_0} \quad (1)$$

$$\frac{\partial h}{\partial t} + \nabla \cdot (H\mathbf{u}) = 0, \quad (2)$$

where $\mathbf{u}$ is the upper layer horizontal velocity vector, $\mathbf{k}$ the unit upward vector, the reduced gravity constant (= 0.03 m s^{-2}), h the upper layer thickness (ULT), H the time-mean ULT (= 320 m), ρ_0 the upper layer density, $\boldsymbol{\tau}$ the surface wind stress vector, and A_h the horizontal eddy viscosity (= 800 m^2 s^{-1}). In this 1½-layer RG model setting, sea level η signals are related to the ULT signals linearly via $\eta = g'h/g$, where g is the gravitational constant. To hindcast the ULT, or sea level, variations, we integrate Equations 1 and 2 using the ECMWF-Interim reanalysis wind stress data from 1979 to 2019 (Dee et al., 2011). The wind stress data have a spatial resolution of

0.75° × 0.75° and a temporal resolution of one day. The 1½-layer RG model has a spatial grid resolution of 0.25° × 0.25°, and the coarser wind stress data are linearly interpolated onto the model grid during its integration.

To evaluate the effects by nonlinear processes, we analyze the output from the Estimating the Circulation and Climate of the Ocean, phase-II (ECCO2) ocean state estimate (Menemenlis et al., 2005a). The ECCO2 model is based on the Massachusetts Institute of Technology General Circulation Model (MITgcm; Marshall et al., 1997), a three-dimensional, z-level, hydrostatic, and Boussinesq global ocean model. The model has a mean horizontal resolution of 18 km and 50 levels in the vertical. The eddy-permitting ocean state estimate is obtained by a least squares fit of the MITgcm to available satellite and in situ data. Using a Green's function approach (Menemenlis et al., 2005b), the least squares fit is employed for a number of model control parameters: initial temperature-salinity conditions, surface boundary conditions, background eddy viscosity and diffusivity, and bottom drag. Using the optimized control parameters, the model is run forward unconstrained as in other prognostic model simulations. For this study, we used the daily-mean sea level and three-day-mean subsurface output of the ECCO2 ocean state estimate from 1992 to 2019. The spatial resolution of the ECCO2 output is 0.25° × 0.25°, the same as the linear 1½-layer RG model described in the preceding paragraph.

Note that the baseline ECCO2 ocean state estimate is forced by the ECMWF reanalysis surface wind stress data. Although these wind stress data are adjusted during the optimization process for control parameters, the adjusted wind stress data are similar to the original wind stress product in the tropical Pacific Ocean of interest here (figure not shown). Because the same ECMWF wind stress data are used to drive the linear 1½-layer RG model, throughout this study we will use the ECCO2 ocean state estimate to represent the total (sum of linear and nonlinear) response of the tropical Pacific Ocean and that of the linear 1½-layer RG model, its linear response. Thus defined, the difference between the two models represents the effects resulting from the nonlinear processes.

RESULTS FROM LINEAR AND NONLINEAR MODEL SIMULATIONS

Time-varying sea level, a vertically integrated quantity, can effectively quantify the relative contributions of linear and nonlinear processes in the tropical western Pacific Ocean. Sea level has also the advantage of being monitored and gridded globally by concurrent satellite altimeter missions. For this study, we use the global sea level anomaly data set produced by SSALTO/Data Unification and Altimeter Combination System (DUACS) and distributed by AVISO (http://www.aviso.oceanobs.com). This data set merges along-track sea level measurements from all available satellite altimeter missions after 1993 and has a daily temporal resolution and a 1/4°-longitude Mercator spatial resolution from January 1993 to April 2019.

Figure 2 compares the sea level time series at (a) Kwajalein, (b) Pohnpei, (c) Yap, and (d) Palau, respectively (see Figure 1a for their locations). In all plots,

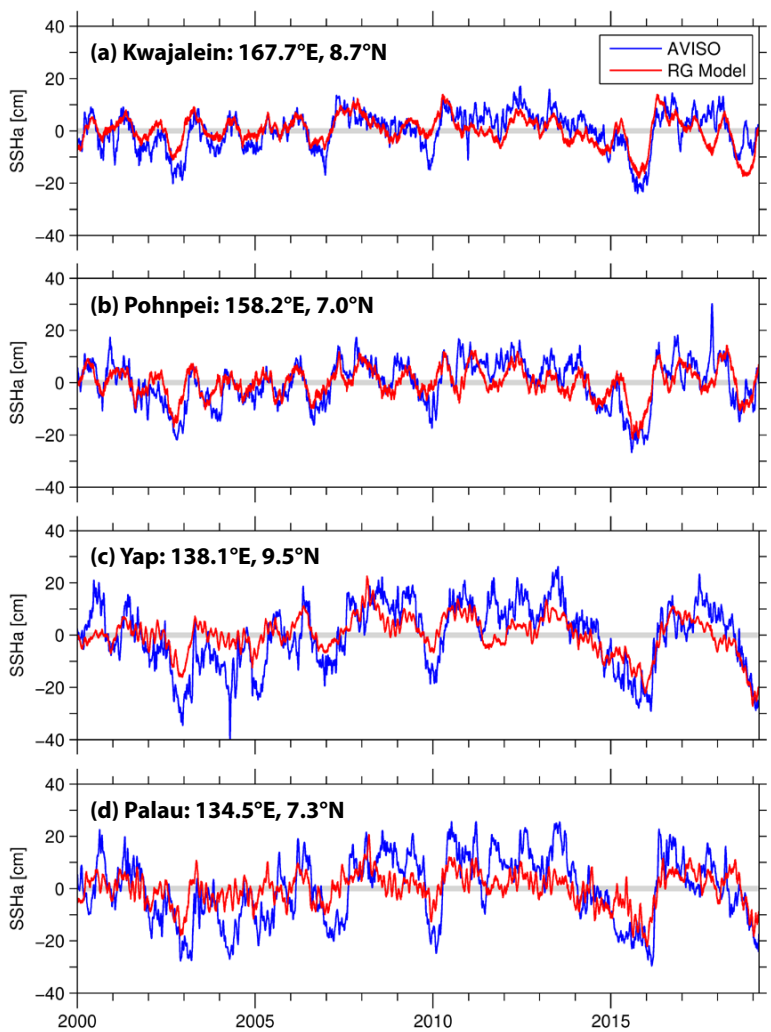

FIGURE 2. Comparisons of sea level anomalies between AVISO (blue lines) and the wind-forced 1½-layer reduced-gravity (RG) model output (red lines) at (a) Kwajalein, (b) Pohnpei, (c) Yap, and (d) Palau. See Figure 1a for their geographical locations. The same comparisons between AVISO and the Estimating the Circulation and Climate of the Ocean, Phase II (ECCO2) model output can be found in Figure S1 in the online supplementary materials.

blue lines denote the altimeter-measured sea level time series compiled by AVISO, and red lines denote the results from the linear 1½-layer RG model based on $\eta = g'h/g$ from Equations 1 and 2. Visually, there is a distinction between Kwajalein/Pohnpei east of 150°E and Yap/Palau west of 150°E: at the two eastern locations, the modeled sea level variability exhibits an amplitude similar to the observations. The root-mean-squared (rms) differences between the observed and modeled sea level at Kwajalein and Pohnpei are 5.4 cm and 5.9 cm, respectively. At Yap and Palau, on the other hand, the modeled sea level signals tend to underestimate the observed signals, and the rms sea level differences at these two locations are 8.7 cm and 10.1 cm, respectively. In other words, while the linear vorticity dynamics does an effective job of simulating the wind-forced sea level variability east of 150°E in the tropical Pacific Ocean, it does a poor job of hindcasting the observed sea level variability west of 150°E, and this is particularly true for Palau.

To clarify the reasons behind the poor performance by the linear 1½-layer RG model, we focus below on the evolution of sea level and upper ocean circulation around Palau during the El Niño to La Niña transition in early 2016. In contrast to the gradual sea level rise of 0.3 m over the January–June period at Palau from the linear 1½-layer RG model (Figure 3a), the nonlinear ECCO2 simulation favorably captures the observed 0.5 m increase in sea level at Palau over the shorter March–April period (Figure 3b). In order to better understand the processes relevant for this sharp sea level rise event during March–April 2016, we plot in Figure 4 (left column) a sequence of upper ocean horizontal velocity maps from the ECCO2 ocean state estimate and contrast them to the same velocity maps derived from the linear 1½-layer RG model (right column). For the ECCO2 results, the upper ocean is defined as the layer overlying the 26.8 σ_θ isopycnal surface that defines the base of the main thermocline (e.g., Qiu et al., 2015).

As the 2015/16 El Niño event matures in early 2016 (Figure 3c), the tropical Pacific trade winds start to rebound and strengthen in January–February (e.g., L'Heureux et al., 2017; their Figure 4a). The strengthened trade winds generate downward Ekman pumping velocities across the tropical Pacific basin and induce downwelling baroclinic Rossby waves that propagate westward at 0.45 m s^{-1} along the Palau latitude of ~7.3°N. As these upwelling baroclinic Rossby waves arrive at the western Pacific basin, they play two roles that show up in the results of Figures 3 and 4. First, they shift the NECC northward and induce sea level rise throughout the western Pacific Ocean. This linear process via wind-forced baroclinic Rossby waves is captured by the linear 1½-layer RG model (Figure 3a). As they propagate into the western Pacific, the sequence in Figure 4 (left column) reveals that the baroclinic Rossby waves can interact nonlinearly with the pre-existing NECC. Specifically, in late February 2016 (Figure 4b), the incoming downwelling Rossby waves are seen to undulate the zonally aligned NECC that existed in early February (Figure 4a). As time progresses, the downwelling Rossby waves increase the amplitude of the undulating NECC (Figure 4c), resulting in NECC impingement upon Palau directly from

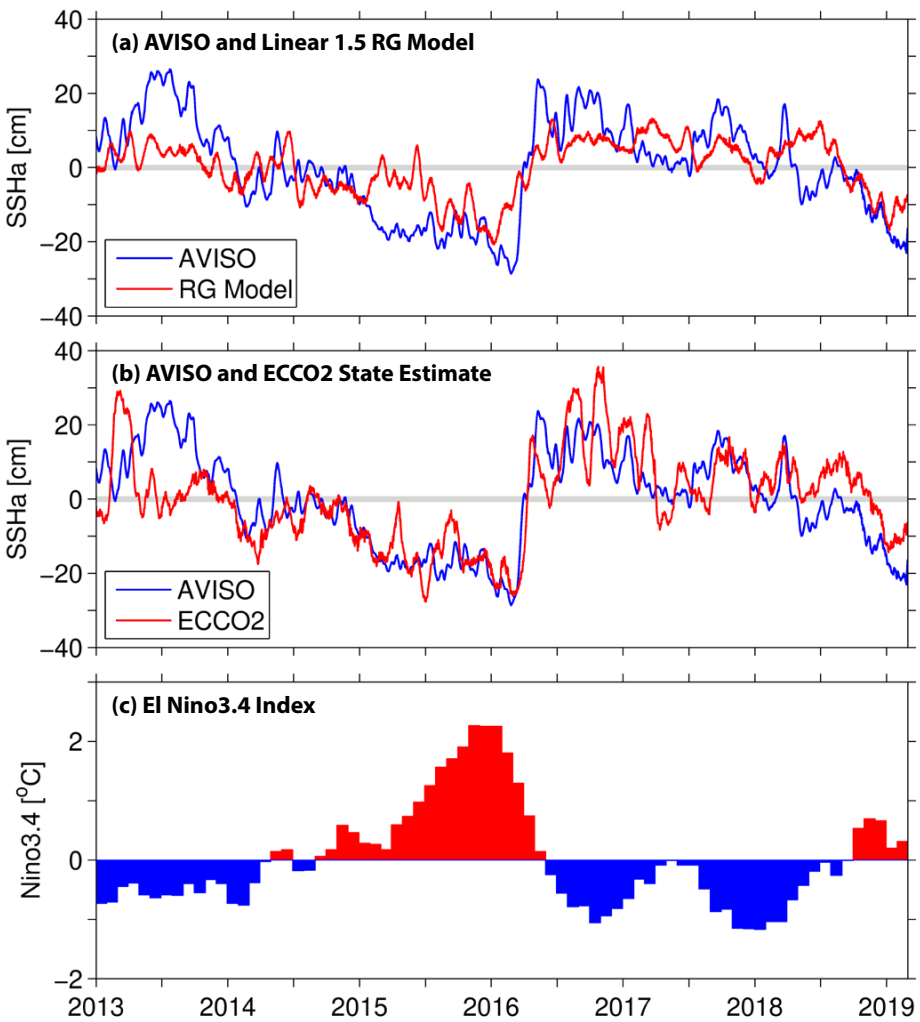

FIGURE 3. Comparisons between the observed versus modeled sea level anomalies at Palau (a) between AVISO and the wind-forced 1½-layer RG model and (b) between AVISO and the ECCO2 ocean state estimate for the 2013–2019 period. (c) Time series of the Niño-3.4 index.

the southwest in mid-April (Figure 4d). It is the combined effects of the linearly forced northward shift of the NECC and the nonlinearly forced amplification of its undulation that generates the intense northward flows around Palau (recall Figure 1d), resulting in sharp water temperature and sea level increases detected at Palau, as shown in Figure 1b–c. By May 2016, the northward shifted NECC breaks down to the east of Palau (Figure 4e–f), and, as may be inferred from the oscillating sea level signals in Figure 3b and the sequential maps of Figure S2 in the online supplementary materials, the NECC does not begin to return to normalcy until early 2017.

Without the inclusion of nonlinear interaction between the Rossby waves and the pre-existing background circulation, the NECC in the linear 1½-layer RG model behaves laminarly and exhibits a gradual northward shift over the February–May period in 2016 (Figure 4, right column). Accompanying this northward shift, the NECC in the linear model shows a progressive weakening, but it does not disintegrate as seen in the nonlinear ECCO2 model.

In this section, we have focused on the linear versus nonlinear evolutions of the NECC during the 2016 El Niño to La Niña transition. Very similar behaviors of the NECC have also been detected during the 1998 El Niño to La Niña transition. Interested readers are referred to Figures S3 and S4 for details.

DYNAMICS OF THE NONLINEAR PROCESSES

To evaluate the geographical dependence of the nonlinear processes described in the preceding section, we plot in Figure 5a the upper ocean eddy kinetic energy (EKE) distribution in the tropical western Pacific Ocean based on the ECCO2 ocean state estimate. As may be expected, the EKE distribution is highly spatially inhomogeneous. High EKE values are concentrated in the region south and southwest of Palau. This region, where the Mindanao and Halmahera

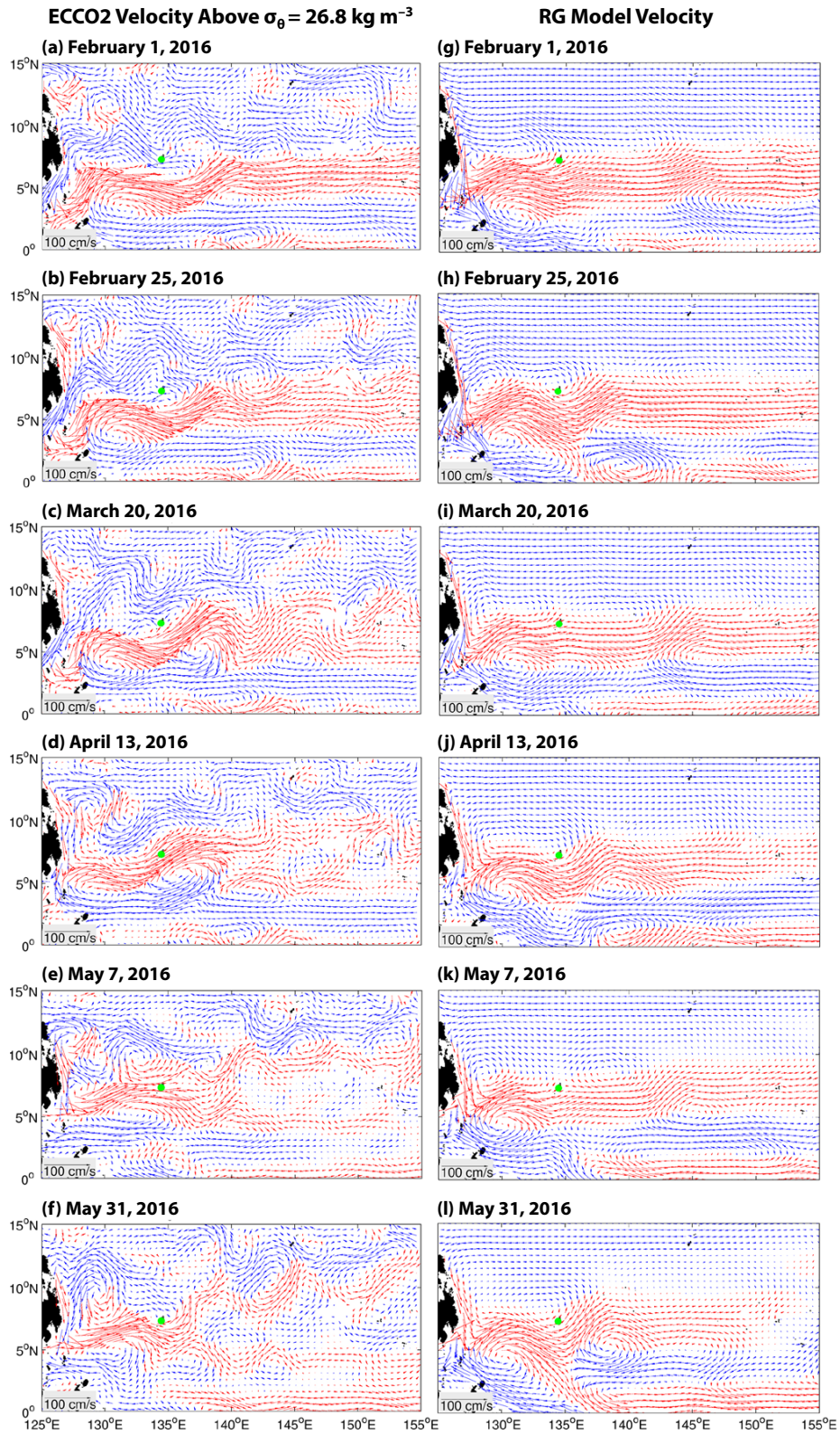

FIGURE 4. (left column) Evolution of the upper ocean velocity fields from the ECCO2 ocean state estimate on (a) February 1, (b) February 25, (c) March 20, (d) April 13, (e) May 7, and (f) May 31, 2016. Velocity vectors with an eastward (westward) component are plotted in red (blue). (right column) Same as left column except for the upper ocean velocity field from the wind-forced 1½-layer RG model output.

eddies reside, includes the poleward-flowing New Guinea Coastal Current, the equatorward-flowing Mindanao Current along the Philippine coast, and the eastward-flowing NECC (e.g., Qiu and Lukas, 1996; Heron et al., 2006; Kashino et al., 2013; Hu et al., 2015; Schönau and Rudnick, 2017). It is worth emphasizing that the EKE value shown in Figure 5a is related to the local Rossby number Ro via $\mathrm{Ro} = \sqrt{EKE}/\beta L_R^2$, where β is the meridional gradient of the Coriolis parameter and L_R the baroclinic Rossby radius of deformation. Given that L_R in the region of our interest is about 150 km (Chelton et al., 1998), an EKE value of 0.01~0.1 $m^2\ s^{-2}$ in the Mindanao and Halmahera eddies region leads to Ro = 0.20~0.64, suggesting the importance of local nonlinear processes when the regional EKE level is elevated.

It is important to note that the EKE level, or the local Rossby number, is time dependent. For example, the blue line in Figure 5b shows the upper ocean EKE time series averaged in the area of 130°–135°E and 3°–8°N southwest of Palau from 2013 to 2019. The EKE level in this region can modulate significantly, with peak values that may exceed three times the mean EKE value. In particular, during the latter half of 2015 when El Niño entered its mature phase and during April of 2016 when the wind-forced downwelling Rossby waves broke down the NECC (recall Figure 4d), EKE levels around Palau were at maximum levels in the six years of data shown. Notice that the interannual EKE modulations mentioned above have much larger amplitudes than those associated with the climatological seasonal changes of the NECC (red line in Figure 5b; Chen et al., 2015). In other words, the large EKE signals detected in the latter half of 2015 and in April 2016 should not be considered due to wind-forced seasonal fluctuations of the NECC.

One way to quantify the relative importance of nonlinear processes is to examine the continuity equation through the Reynolds decomposition as follows:

$$\frac{\partial h'}{\partial t} = -\nabla\cdot(\boldsymbol{u}'\overline{h}) - \nabla\cdot(\overline{\boldsymbol{u}}h') - \nabla\cdot(\boldsymbol{u}'h'), \quad (3)$$

where h' and $\boldsymbol{u}'$ denote the anomalies of the upper layer thickness and velocity from their time-mean values $\overline{h}$ and $\overline{\boldsymbol{u}}$, respectively. The first two terms on the right-hand side of Equation 3 signify the linear processes of the anomalous flow advecting the mean ULT and the mean flow advecting the anomalous ULT. In contrast, the last term in Equation 3 represents the nonlinear interaction between the anomalous flow and the ULT fields. In Figure 6a, we plot the rms amplitude ratio of nonlinear versus linear process terms in Equation 3. Consistent with the distribution map in Figure 5a, this ratio is spatially inhomogeneous and the nonlinear processes become more prominent where the regional EKE level is higher. Figure 6b,c compares the time series of $\partial h'/\partial t$ to the $-\nabla\cdot(\boldsymbol{u}'\overline{h}) - \nabla\cdot(\overline{\boldsymbol{u}}h')$ versus $-\nabla\cdot(\boldsymbol{u}'h')$ terms in the region of 3°–8°N and 130°–135°E during 2013–2019. While in many instances the local rate of change of h' is determined by the linear processes (the blue curve in Figure 6c), the nonlinear term plays a predominant role in periods when the local EKE level is high, for example, in the second half of 2015 and in April 2016.

To clarify the energy sources that lead to the time-varying EKE level in the region of interest, we plot in Figure 7a,b the upper ocean baroclinic and baro-

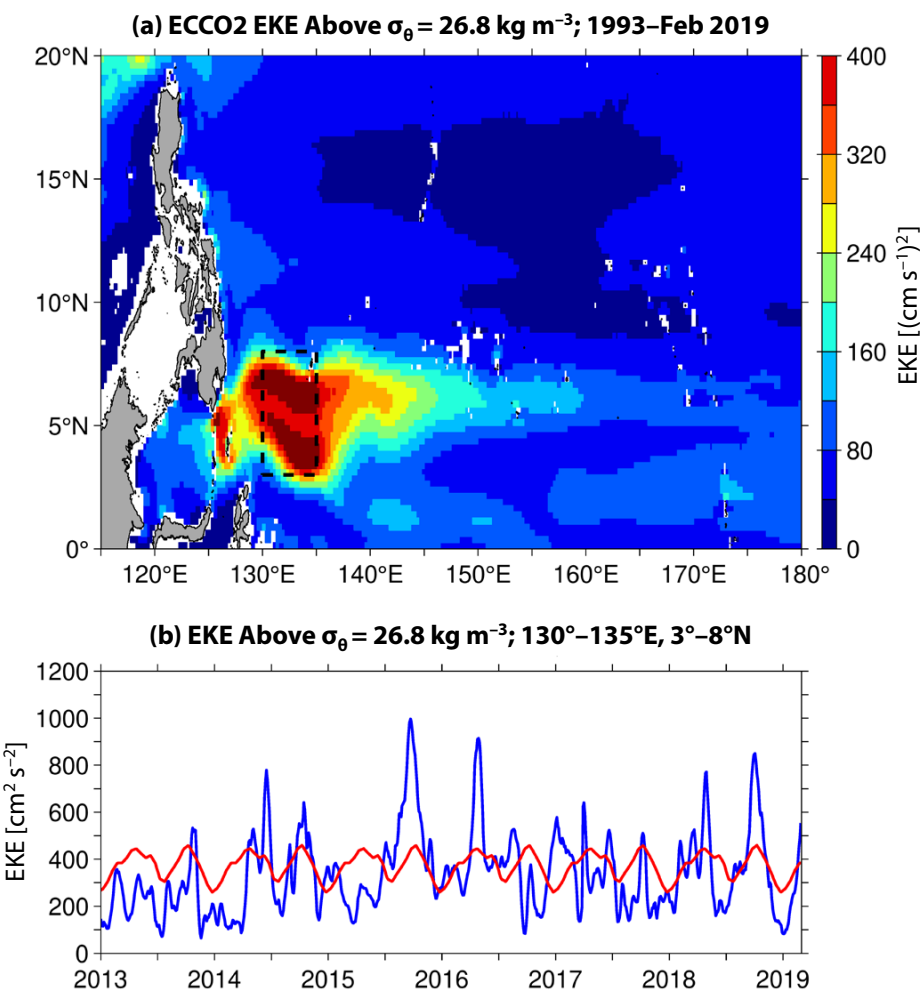

FIGURE 5. (a) Upper ocean eddy kinetic energy (EKE) distribution from the ECCO2 ocean state estimate of 1993–2019. (b) Time series of EKE averaged in the region southwest of Palau at 3°–8°N and 130°–135°E from 2013 to 2019 (blue line). Red line shows the climatological EKE time series in the same region. The EKE climatology here is formed over the period 1993–2018.

tropic EKE conversion rate maps based on the ECCO2 ocean state estimate. Here the two conversion rates are defined by:

$$\text{baroclinic conversion rate} = -\frac{g}{\rho_0}(\rho' w'), \quad (4)$$

and

$$\text{barotropic conversion rate} = -(u_i' u_j')\frac{\partial \overline{u}_i}{\partial x_j}, \quad (5)$$

where ρ' and w' denote the potential density and vertical velocity anomalies from their respective time means, and summations over the repeated indices i and j are assumed in Equation 5. Physically, Equation 4 indicates the conversion from eddy potential energy to EKE, and a negative $\rho' w'$ value indicates lighter (heavier) water is transported upward (downward); this reduces the available potential energy of the mean state and is the source for baroclinic instability. Similarly, Equation 5 represents the conversion from mean kinetic energy to eddy kinetic energy through Reynolds stresses and is the cause for barotropic instability. In the region southwest of Palau, Figure 7a,b reveals that the regional EKE variability derives its energy source from the mean shear of the NECC via barotropic instability. This energetics result, in regard to NECC's barotropic instability being the primary energy source for EKE in the Mindanao and Halmahera eddies region, agrees with our recent study based on the eddy-resolving global OFES (OGCM for Earth Simulator) output independent of the ECCO2 ocean state estimate (Qiu et al., 2015; see their Figure 13).

Finally, a look at temporal variations in the barotropic conversion rate in the region of 3°–8°N and 130°–135°E (red line in Figure 7c) indicates that they match favorably with those of the regional EKE level shown by the blue line in Figure 5b. Specifically, the barotropic conversion rate is high during the latter half of 2015 and the first half of 2016 when the regional EKE level was unseasonably high. This confirms that the energy source for eddy variability around Palau is the horizontally sheared NECC via barotropic instability.

SUMMARY

Wind-forced linear baroclinic Rossby wave adjustment is a useful dynamical framework for understanding and exploring the low-frequency variability in the tropical Pacific Ocean. However, in the region surrounding and southwest of Palau, this dynamical framework fails to capture upper ocean variability with timescales shorter than O(100 days). These short-term variations can result in large-amplitude fluctuations in sea level, upper ocean temperatures, and anomalous northward flows exceeding 0.5 m, 10°C, and 0.5 m s^{-1}, respectively, over a period of one to two months around Palau. Although we have focused on the 2015/16 El Niño event in this study, sim-

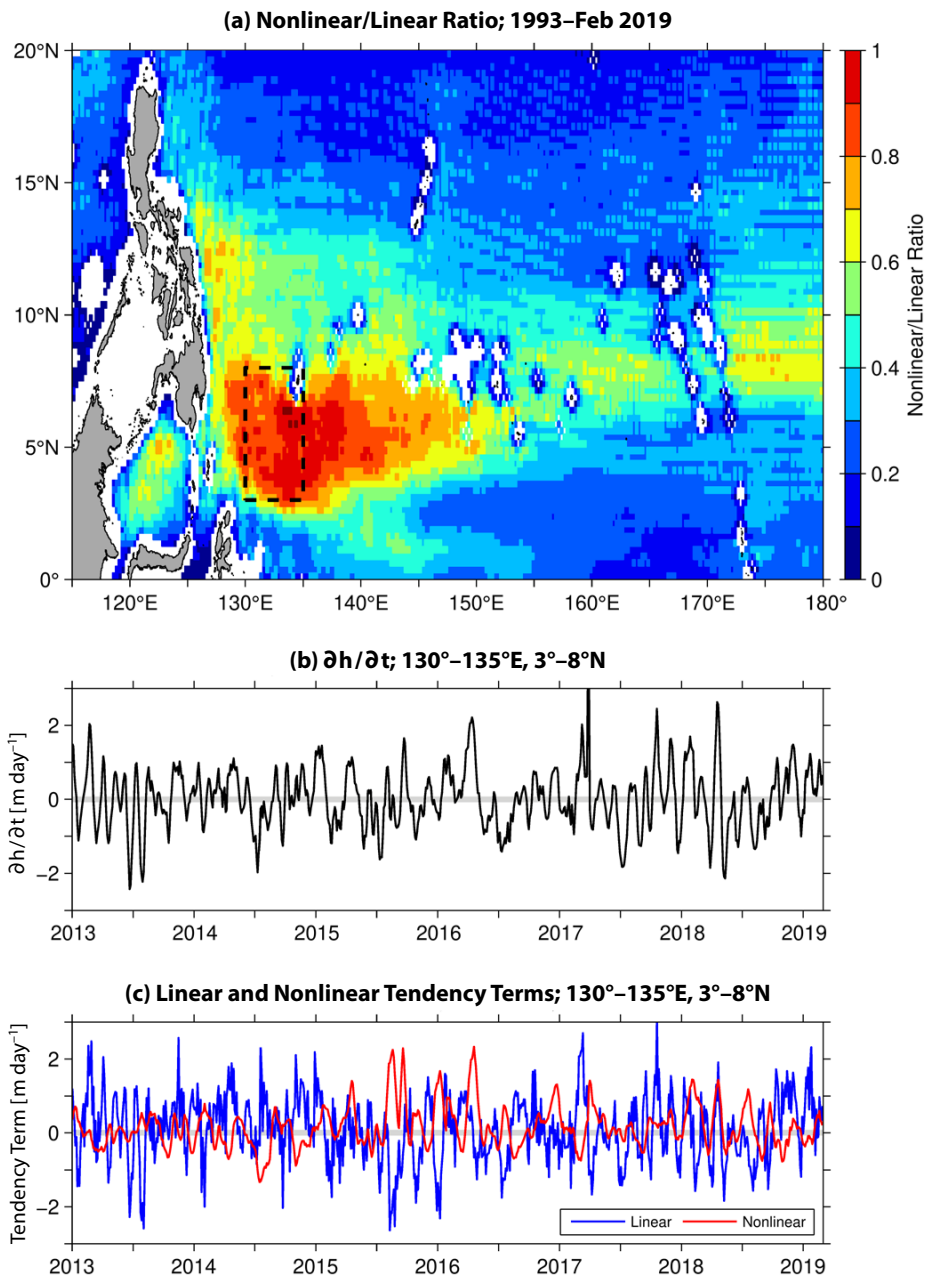

FIGURE 6. (a) Ratio of the rms amplitude of the nonlinear term over that of the linear term in Equation 3 from the upper ocean ECCO2 ocean state estimate. (b) Time series of the term in Equation 3 in the region southwest of Palau at 3°–8°N and 130°–135°E during 2013–2019. (c) Same as (b) except for the nonlinear term (red line) and the linear term (blue line).

ilar large-amplitude sea level changes were detected during the El Niño to La Niña transition periods in the springs of 1998 and 2010.

Dynamically, these large-amplitude upper ocean circulation fluctuations are a result of nonlinear interaction. Specifically, as an El Niño event terminates and transitions to a La Niña phase, the tropical trade winds rebound, generating downwelling baroclinic Rossby waves across the off-equatorial North Pacific basin. As these wind-forced downwelling baroclinic Rossby waves propagate westward into the tropical western basin, they modulate the pre-existing NECC and induce large-amplitude eddy perturbations. Rather than extracting energy from the regional available potential energy (APE), eddy perturbations grow by reducing the lateral shear of the pre-existing NECC. It is these nonlinear eddy perturbations resulting from barotropic instability that are responsible for the short-term, large-amplitude sea level/upper ocean temperature increase and anomalous northward flows around Palau.

We have clarified in this study the nonlinear processes underlying the short-term upper ocean circulation variability in the western tropical Pacific Ocean. As large-amplitude eddy perturbations such as those observed in 2016 can last over a period of nine months (see Figures 4 and S2), they can likely affect the upper ocean heat and salt budgets and may induce enhanced lateral and vertical water mass exchanges in this region. It will be important for future studies to explore the consequences of the nonlinear NECC and the wind-forced baroclinic Rossby wave interactions from water mass exchange and heat/salt budget perspectives, as well as how a rapidly evolving physical environment can affect coral reef ecology and marine ecosystems.

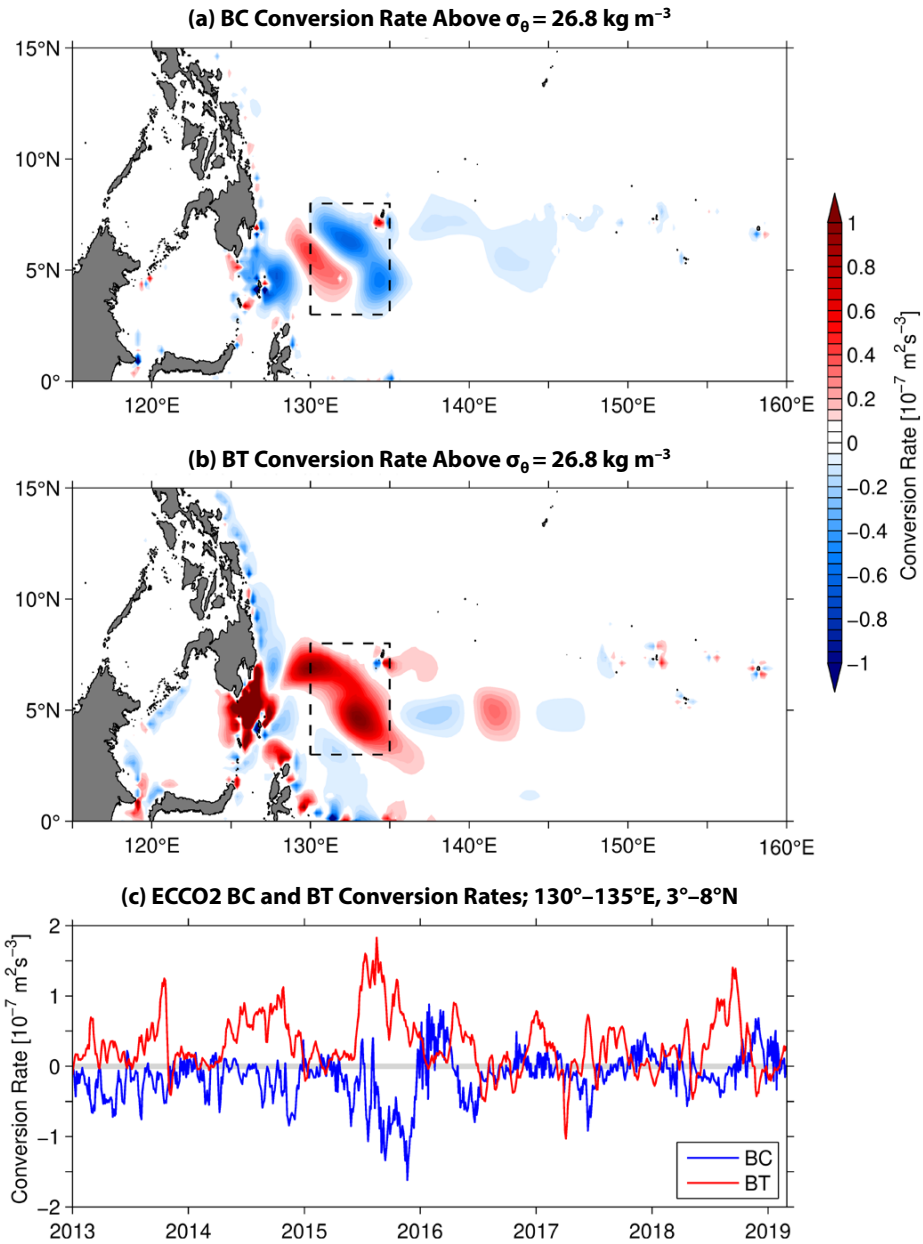

FIGURE 7. Distributions of (a) baroclinic conversion rate and (b) barotropic conversion rate from the upper ocean ECCO2 ocean state estimate. (c) Time series of the baroclinic (blue line) and barotropic (red line) conversion rates in the region southwest of Palau at 3°–8°N and 130°–135°E from 2013 to 2019.

SUPPLEMENTARY MATERIALS

Supplementary Figures S1–S4 are available online at https://doi.org/10.5670/oceanog.2019.408.

REFERENCES

Andres, M., M. Siegelman, V. Hormann, R.C. Musgrave, S.T. Merrifield, D.L. Rudnick, M.A. Merrifield, M.H. Alford, G. Voet, H.W. Wijesekera, and others. 2019. Eddies, topography, and the abyssal flow by the Kyushu-Palau Ridge near Velasco Reef. *Oceanography* 32(4):46–55, https://doi.org/10.5670/oceanog.2019.410.

Bruno, J.F., C.E. Siddon, J.D. Whiman, P.L. Colin, and M.A. Toscano. 2001. El Niño related coral bleaching in Palau, western Caroline Islands. *Coral Reefs* 20:127–136, https://doi.org/10.1007/s003380100151.

Cabrera, O.C., C.L. Villanoy, I.D. Alabia, and A.L. Gordon. 2015. Shifts in chlorophyll *a* associated with the North Equatorial Current bifurcation latitude off eastern Luzon. *Oceanography* 28(4):46–53, https://doi.org/10.5670/oceanog.2015.80.

Chelton, D.B., R.A. de Szoeke, M.G. Schlax, K.E. Naggar, and N. Siwertz. 1998. Geographical variability of the first baroclinic Rossby radius of deformation. *Journal of Physical Oceanography* 28:433–460, https://doi.org/10.1175/1520-0485(1998)028<0433:GVOTFB>2.0.CO;2.

Chen, X., B. Qiu, S. Chen, Y. Qi, and Y. Du. 2015. Seasonal eddy kinetic energy modulations along the North Equatorial Countercurrent in the western Pacific. *Journal of Geophysical Research* 120:6,351–6,362, https://doi.org/10.1002/2015JC011054.

Colin, P.L. 2009. *Marine Environments of Palau*. Indo-Pacific Press, 414 pp., https://coralreefpalau.org/wp-content/uploads/2017/04/Colin-PL-2009-Marine-Environments-of-Palau.pdf.

Colin, P.L. 2018. Ocean warming and the reefs of Palau. *Oceanography* 31(2):126–135, https://doi.org/10.5670/oceanog.2018.214.

Dee, D.P., S.M. Uppala, A.J. Simmons, P. Berrisford, P. Poli, S. Kobayashi, U. Andrae, M.A. Balmaseda, G. Balsamo, P. Bauer, and others. 2011. The ERA-Interim reanalysis: Configuration and performance of the data assimilation system. *Quarterly Journal of the Royal Meteorological Society* 137:553–597, https://doi.org/10.1002/qj.828.

Gill, A.E. 1982. *Atmosphere-Ocean Dynamics*. International Geophysics Series, vol. 30, Academic Press, 662 pp.

Greatbatch, R.J., X. Zhu, and M. Class. 2018. Reconstructing tropical Pacific sea level variability for the period 1961–2002 using a linear multimode model. *Journal of Geophysical Research* 123:2,037–2,048, https://doi.org/10.1002/2017JC013652.

Heron, S.F., E.J. Metzger, and W.J. Skirving. 2006. Seasonal variations of the ocean surface circulation in the vicinity of Palau. *Journal of Oceanography* 62:413–426, https://doi.org/10.1007/s10872-006-0065-3.

Hsin, Y.-C., and B. Qiu. 2012. Seasonal fluctuations of the surface North Equatorial Countercurrent (NECC) across the Pacific basin. *Journal of Geophysical Research* 117, C06001, https://doi.org/10.1029/2011JC007794.

Hu, D., L. Wu, A. Sen Gupta, A. Ganachaud, B. Qiu, A.L. Gordon, X. Lin, Z. Chen, S. Hu, G. Wang, and others. 2015. Pacific western boundary currents and their roles in climate. *Nature* 522:299–308, https://doi.org/10.1038/nature14504.

Kashino, Y., A. Atmadipoera, Y. Kuroda, and Lukijanto. 2013. Observed features of the Halmahera and Mindanao Eddies. *Journal of Geophysical Research* 118:6,543–6,560, https://doi.org/10.1002/2013JC009207.

Kessler, W.S. 1990. Observation of long Rossby waves in the northern tropical Pacific. *Journal of Geophysical Research* 95:5,183–5,217, https://doi.org/10.1029/JC095iC04p05183.

Kessler, W.S., and S. Cravatte. 2013. ENSO and short-term variability of the South Equatorial Current entering the Coral Sea. *Journal of Physical Oceanography* 43:956–969, https://doi.org/10.1175/JPO-D-12-0113.1.

L'Heureux, M., K. Takahashi, A.B. Watkins, A.G. Barnston, E.J. Becker, T.E. Di Liberto, F. Gamble, J. Gottschalck, M.S. Halpert, B. Huang, and others. 2017. Observing and predicting the 2015/16 El Niño. *Bulletin of the American Meteorological Society* 88:1,363–1,382, https://doi.org/10.1175/BAMS-D-16-0009.1.

Marshall, J., A. Adcroft, C. Hill, L. Perelman, and C. Heisey. 1997. A finite-volume, incompressible Navier Stokes model for studies of the ocean on parallel computers. *Journal of Geophysical Research* 102:5,753–5,766, https://doi.org/10.1029/96JC02775.

Menemenlis, D., C. Hill, A. Adcroft, J.-M. Campin, B. Cheng, B. Ciotti, I. Fukumori, P. Heimbach, C. Henze, A. Köhl, and others. 2005a. NASA supercomputer improves prospects for ocean climate research. *Eos Transactions, American Geophysical Union* 86:89–96, https://doi.org/10.1029/2005EO090002.

Menemenlis, D., I. Fukumori, and T. Lee. 2005b. Using Green's functions to calibrate an ocean general circulation model. *Monthly Weather Review* 133:1,224–1,240, https://doi.org/10.1175/MWR2912.1.

Qiu, B., and S. Chen. 2010. Interannual-to-decadal variability in the bifurcation of the North Equatorial Current off the Philippines. *Journal of Physical Oceanography* 40:2,525–2,538, https://doi.org/10.1175/2010JPO4462.1.

Qiu, B., and S. Chen. 2012. Multi-decadal sea level and gyre circulation variability in the northwestern tropical Pacific Ocean. *Journal of Physical Oceanography* 42:193–206, https://doi.org/10.1175/JPO-D-11-061.1.

Qiu, B., and T.M. Joyce. 1992. Interannual variability in the mid- and low-latitude western North Pacific. *Journal of Physical Oceanography* 22:1,062–1,079, https://doi.org/10.1175/1520-0485(1992)022<1062:IVITMA>2.0.CO;2.

Qiu, B., and R. Lukas. 1996. Seasonal and interannual variability of the North Equatorial Current, the Mindanao Current, and the Kuroshio along the Pacific western boundary. *Journal of Geophysical Research* 101:12,315–12,330, https://doi.org/10.1029/95JC03204.

Qiu, B., S. Chen, D. Rudnick, and Y. Kashino. 2015. A new paradigm for the North Pacific subthermocline low-latitude western boundary current system. *Journal of Physical Oceanography* 45:2,407–2,423, https://doi.org/10.1175/JPO-D-15-0035.1.

Rio, M.-H., S. Mulet, and N. Picot. 2014. Beyond GOCE for the ocean circulation estimate: Synergetic use of altimetry, gravimetry, and in situ data provides new insight into geostrophic and Ekman currents. *Geophysical Research Letters* 41:8,918–8,925, https://doi.org/10.1002/2014GL061773.

Schönau, M.C., and D.L. Rudnick. 2017. Mindanao Current and undercurrent: Structure and transport from repeat glider observations. *Journal of Physical Oceanography* 47:2,055–2,075, https://doi.org/10.1175/JPO-D-16-0274.1.

Schönau, M.C., H.W. Wijesekera, W.J. Teague, P.L. Colin, G. Gopalakrishnan, D.L. Rudnick, B.D. Cornuelle, Z.R. Hallock, and D.W. Wang. 2019. The end of an El Niño: A view from Palau. *Oceanography* 32(4):32–45, https://doi.org/10.5670/oceanog.2019.409.

Schramek, T.A., P.L. Colin, M.A. Merrifield, and E.J. Terrill. 2018. Depth-dependent thermal stress around corals in the tropical Pacific Ocean. *Geophysical Research Letters* 45:9,739–9,747, https://doi.org/10.1029/2018GL078782.

Timmermann, A., S. McGrager, and F.-F. Jin. 2010. Wind effects on the past and future regional sea level trends in the southern Indo-Pacific. *Journal of Climate* 23:4,429–4,437, https://doi.org/10.1175/2010JCLI3519.1.

Zedler, S.E., B.S. Powell, B. Qiu, and D.L. Rudnick. 2019. Energy transfer in the western tropical Pacific. *Oceanography* 32(4):136–145, https://doi.org/10.5670/oceanog.2019.419.

Zhuang, W., B. Qiu, and Y. Du. 2013. Low-frequency western Pacific Ocean sea level and circulation changes due to the connectivity of the Philippine archipelago. *Journal of Geophysical Research* 118:6,759–6,773, https://doi.org/10.1002/2013JC009376.

ACKNOWLEDGMENTS

This study was supported by the ONR project Flow Encountering Abrupt Topography (FLEAT): N00014-15-1-2315 (BQ and SC), N00014-15-1-2600 (BP), and N00014-15-1-2488 (DR and MS). Water temperature monitoring efforts in Palau were supported by the staff of the Coral Reef Research Foundation through internal funds. We thank the Palau National Government for permission to carry out the research in Palau.

AUTHORS

Bo Qiu (bo@soest.hawaii.edu) is Professor, **Shuiming Chen** is Senior Researcher, and **Brian S. Powell** is Professor, all in the Department of Oceanography, University of Hawai'i at Mānoa, Honolulu, HI, USA. **Patrick L. Colin** is Director, Coral Reef Research Foundation, Koror, Palau. **Daniel L. Rudnick** is Professor, Scripps Institution of Oceanography, University of California San Diego, La Jolla, CA, USA. **Martha C. Schönau** is Senior Scientist, Applied Ocean Sciences, Fairfax Station, VA, USA.

ARTICLE CITATION

Qiu, B., S. Chen, B.S. Powell, P.L. Colin, D.L. Rudnick, and M.C. Schönau. 2019. Nonlinear short-term upper ocean circulation variability in the tropical western Pacific. *Oceanography* 32(4):22–31, https://doi.org/10.5670/oceanog.2019.408.

COPYRIGHT & USAGE

This is an open access article made available under the terms of the Creative Commons Attribution 4.0 International License (https://creativecommons.org/licenses/by/4.0/), which permits use, sharing, adaptation, distribution, and reproduction in any medium or format as long as users cite the materials appropriately, provide a link to the Creative Commons license, and indicate the changes that were made to the original content.